A novel enhancement mode AlGaN/GaN high electron mobility transistor with split floating gates*

Hui Wang(王辉)[1,2], Ning Wang(王宁)[1,2], Ling-Li Jiang(蒋苓利)[1,2], Xin-Peng Lin(林新鹏)[1,2], Hai-Yue Zhao(赵海月)[1,2], and Hong-Yu Yu(于洪宇)[1,2,†]

[1] Department of Electrical and Electronic Engineering, Southern University of Science and Technology, Shenzhen 518055, China
[2] Shenzhen Key Laboratory of the Third Generation Semiconductor, Shenzhen 518055, China

(Received 1 November 2016; revised manuscript received 8 January 2017; published online 20 February 2017)

A novel enhancement-mode AlGaN/GaN high electron mobility transistor (HEMT) is proposed and studied. Specifically, several split floating gates (FGs) with negative charges are inserted to the conventional MIS structure. The simulation results revealed that the V_{th} decreases with the increase of polarization sheet charge density and the tunnel dielectric (between FGs and AlGaN) thickness, while it increases with the increase of FGs sheet charge density and blocking dielectric (between FGs and control gate) thickness. In the case of the same gate length, the V_{th} will left shift with decreasing FG length. More interestingly, the split FGs could significantly reduce the device failure probability in comparison with the single large area FG structure.

Keywords: AlGaN/GaN, high electron mobility transistor, split floating gates, enhancement mode

PACS: 73.40.Kp, 81.05.Ea, 85.30.De, 85.30.Tv **DOI:** 10.1088/1674-1056/26/4/047305

1. Introduction

Enhancement-mode (E-mode) AlGaN/GaN HEMTs with a large positive threshold voltage ($V_{th} > 2$ V) are strongly desired for high voltage, high power and high frequency switching applications.[1] In the last few years, major efforts in the development of E-mode HEMTs have been witnessed.[2] These technologies mainly include fluorine[3,4] or oxygen[5] ion implantation, P-type GaN or AlGaN gate,[6] recess gate etching,[7–9] and piezo neutralization,[10] etc. However, concerns associated with the above-mentioned technologies such as large gate leakage current owing to the process damage to the channel, difficulties of preparation process, and small resultant V_{th} still have not been addressed completely.

Floating gates (FGs), usually applied in flash memory devices, have recently been proposed and experimentally confirmed to be a promising approach to obtain E-mode by way of charge storing without reducing the channel conductance.[11,12] The main shortcomings are the requirement of large FG sheet charge density as well as charge retention limitation which affects the V_{th} stability. Although Huang *et al.*[13] reported that the FG sheet charge density can be lowered by combining FG and gate recess etching, the charge retention still remains a problem. It is known that charge loss of a single large area FG due to a weak spot in the dielectric would result in V_{th} dropping to a negative value and hence a catastrophic short-circuit can happen. To mitigate this problem, a novel HEMT with split FGs structure is proposed and studied by simulations in this work.

2. Simulation details

The simulations were carried out with software Silvaco. The key polarization and mobility models used were TEN.POLAR model and Albrecht model, respectively. The V_{th} was studied as a function of polarization-induced sheet charge density (σ), FGs sheet charge density (Q_f), tunnel dielectric (TD), and blocking dielectric (BD) materials and thicknesses. The range of σ was from -2.1×10^{12} cm^{-2} to -9.5×10^{12} cm^{-2}. The ranges of negative Q_f were from -1.0×10^{13} cm^{-2} to -1.5×10^{13} cm^{-2}. SiO_2, Si_3N_4, Al_2O_3, and HfO_2 were applied as both TD and BD. The ranges of TD thickness (t_t) and BD thickness (t_b) were 5 nm$\sim$10 nm and 5 nm$\sim$30 nm, respectively. In the study of FG failure on the V_{th}, 6 FGs when complete charge loss occurs in 0, 1, 2, 3, 4, 5 FGs were studied, the length of each FG (l_f) was equal to 1 μm and their spacing (s_f, the horizontal distance between 2 adjacent FGs) was equal to 0.2 μm. For figuring out the length of single FG on the V_{th}, the FG length of 0.2 μm$\sim$7 μm was studied. In all the simulations of transfer characteristics, the gate metal work function was 4.6 eV and the drain voltage was 1 V. The gate length (l_g) was kept at 7 μm and the gate-to-source spacing (l_{gs}) and gate-to-drain spacing (l_{gd}) were kept at 3 μm. The device schematic is shown in Fig. 1.

*Project supported by "Efficient and Energy-Saving GaN on Si Power Devices" Research Fund (Grant No. KQCX20140522151322946), the Research Fund of the Third Generation Semiconductor Key Laboratory of Shenzhen, China (Grant No. ZDSYS20140509142721434), the "Key Technology Research of GaN on Si Power Devices" Research Fund (Grant No. JSGG20140729145956266), and the "Research of Low Cost Fabrication of GaN Power Devices and System Integration" Research Fund (Grant No. JCYJ201602261926390).

†Corresponding author. E-mail: yuhy@sustc.edu.cn

© 2017 Chinese Physical Society and IOP Publishing Ltd

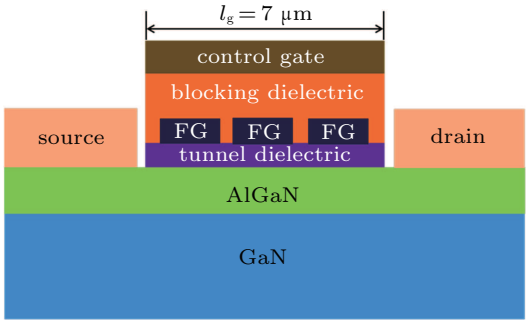


Fig. 1. (color online) Schematic illustration of the HEMT structure with split floating gates (the number of FGs can be adjusted). The gate length (l_g) is 7 μm, the gate-to-source spacing (l_{gs}) and gate-to-drain spacing (l_{gd}) are both 3 μm.

3. Threshold voltage calculation

For conventional MIS HEMTs, the schematic charge distribution and energy band diagram can be seen in Fig. 2(a). The V_{th} can be calculated by Eq. (1)[14]

$$V_{th} = \frac{\Phi_1}{q} - \frac{\Delta E}{q} - \frac{\Phi_2}{q} - \frac{q(t_d)^2}{2\varepsilon_d} n_d - \frac{qt_d}{\varepsilon_d} d_{it} - q\left(\frac{t_d}{\varepsilon_d} + \frac{t_{AlGaN}}{\varepsilon_{AlGaN}}\right)\sigma, \quad (1)$$

where Φ_1 is the metal barrier height for gate/BD, q is the elementary charge, ΔE is the conduction band offset for gate dielectric/GaN, Φ_2 is the conduction band distance from the Fermi-level in GaN, ε_d is the permittivity of gate dielectric, n_d is the average bulk charge of gate dielectric (per unit volume), d_{it} and σ are the sheet charge density at the gate dielectric/AlGaN interface and the AlGaN/GaN-channel interface, respectively.

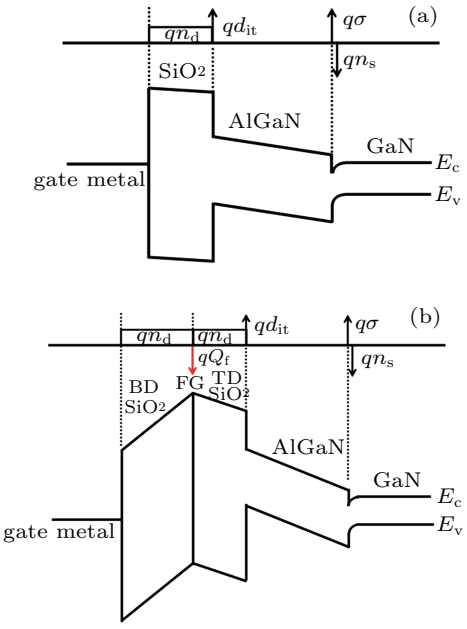


Fig. 2. (color online) Schematic charge distribution and energy band diagram of (a) conventional MIS HEMT and (b) FG HEMT.

While for the FG MIS HEMTs, the schematic charge distribution and energy band diagram can be seen in Fig. 2(b). The V_{th} will be shifted by the FG charge and the V_{th} shift ΔV_{th} is derived in Eq. (2)[15]

$$\Delta V_{th} = -\frac{qt_b}{\varepsilon_b} Q_f. \quad (2)$$

Combining Eqs. (1) and (2), the V_{th} of the FG MIS HEMTs can be calculated by Eq. (3)

$$V_{th} = \frac{\Phi_1}{q} - \frac{\Delta E}{q} - \frac{\Phi_2}{q} - \frac{q(t_b + t_t)^2}{2\varepsilon_d} n_d - \frac{qt_t}{\varepsilon_t} d_{it} - q\left(\frac{t_b + t_t}{\varepsilon_d} + \frac{t_{AlGaN}}{\varepsilon_{AlGaN}}\right)\sigma - \frac{qt_b}{\varepsilon_b} Q_f, \quad (3)$$

where ε_t is the permittivity of TD, ε_b is the permittivity of BD. Since the TD and BD are the same material applied in the simulations, it is known that $\varepsilon_d = \varepsilon_t = \varepsilon_b$. It is also known that n_d, d_{it}, and σ are all positive, and the value of d_{it} increases with the increase of the two-dimensional electron gas (2DEG) sheet charge density (n_s).[14,16] So the V_{th} of the FG MIS HEMTs can be derived as Eq. (4)

$$V_{th} = \frac{\Phi_1}{q} - \frac{\Delta E}{q} - \frac{\Phi_2}{q} - \frac{q(t_b + t_t)^2}{2\varepsilon_d} |n_d| - \frac{qt_d}{\varepsilon_d} |d_{it}| - q\left(\frac{t_b + t_t}{\varepsilon_d} + \frac{t_{AlGaN}}{\varepsilon_{AlGaN}}\right)|\sigma| + \frac{qt_b}{\varepsilon_d} |Q_f|. \quad (4)$$

4. Results and discussions

Figure 3 shows the V_{th} as a function of $|\sigma|$. It is seen that the V_{th} decreases linearly as the $|\sigma|$ increases. In Eq. (4), it is seen that the increase of $|\sigma|$ will lead to the linear decrease of V_{th}. Figure 3 also shows that in the case of the same $|\sigma|$, the V_{th} for $|Q_f|$ is 1.5×10^{13} cm^{-2} is larger than that for $|Q_f|$ is 1×10^{13} cm^{-2}.

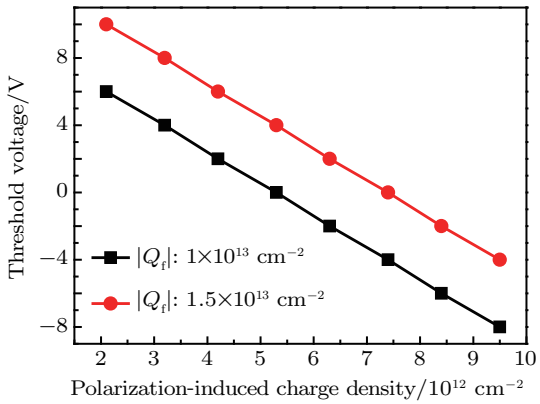


Fig. 3. (color online) The V_{th} as a function of $|\sigma|$. The TD and BD were both SiO_2. The t_t and t_b were 10 nm and 20 nm, respectively. Single FG with l_f of 7 μm (equal to the l_g) was applied.

Figure 4(a) shows that the V_{th} increases linearly with increasing $|Q_f|$, the phenomenon of which is also found in Fig. 3. In Eq. (4), it is seen that when other factors remain unchanged, the V_{th} has a positive linear dependence on $|Q_f|$. As the $|Q_f|$ increases, the V_{th} will increase accordingly. Figure 4(a) also shows that when other factors remain unchanged, the V_{th} decreases when the dielectric changes from lowest-k SiO_2 to

highest-k HfO_2. This variation results from the variation of Φ_1, ΔE, n_d, and ε_d for different dielectrics. Figure 4(b) shows that the V_{th} decreases linearly with the increase of t_t. It is due to the fact that as t_t increases, the V_{th} will decrease since in this situation it is just a function of t_t. Figure 4(c) shows that the V_{th} increases with the increase of t_b. The variation is opposite in comparison with the conventional MIS HEMT in which the V_{th} decreases with the increase gate dielectric (Eq. (1)). Figure 4(c) can also be explained by Eq. (4). It is seen that ΔV_{th} increases with the increase of t_b. Furthermore, the $|Q_f|$ is much larger than other sheet charge density, thus still resulting in the increase of V_{th}. Figure 4(c) also reveals that the $|Q_f|$ can be lowered moderately by increasing t_b.

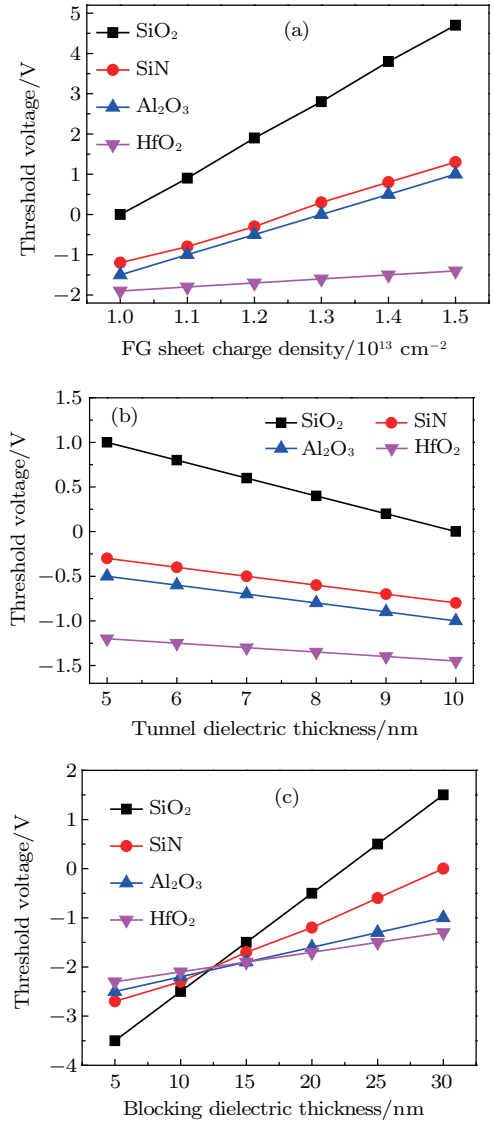


Fig. 4. (color online) (a) The V_{th} as a function of $|Q_f|$. The t_t and t_b were 10 nm and 20 nm, respectively; (b) The V_{th} as a function of t_t. The $|Q_f|$ and t_b were 1×10^{13} cm^{-2} and 20 nm, respectively; (c) The V_{th} as a function of t_b. The $|Q_f|$ and t_t were 1×10^{13} cm^{-2} and 10 nm, respectively. The TD and BD were the same material and the $|n_s|$ is 5.3×10^{12} cm^{-2}. Single FG with l_f of 7 μm (equal to the l_g) was applied.

Figure 5 shows the transfer characteristics of split FG HEMTs when FGs failure is considered. I_d–V_g curves when complete charge loss occurs in 0, 1, 2, 3, 4, 5 FGs of the 6 FG HEMTs are shown for comparison. It is seen that the V_{th} decreases slightly when FGs failure happened, while the reduction (about 0.1 V per FG failure) is still moderate when even 5 FGs failed, implying that the split FGs HEMTs is feasible. It is also noteworthy that the increase of drain current is accompanied with the decrease of V_{th}. Since the drain current increases rather than decreases, which may cause very little impact on the HEMT applications. Figure 5 thus reveals the advantages of the split FGs in comparison with the single large area of FG.

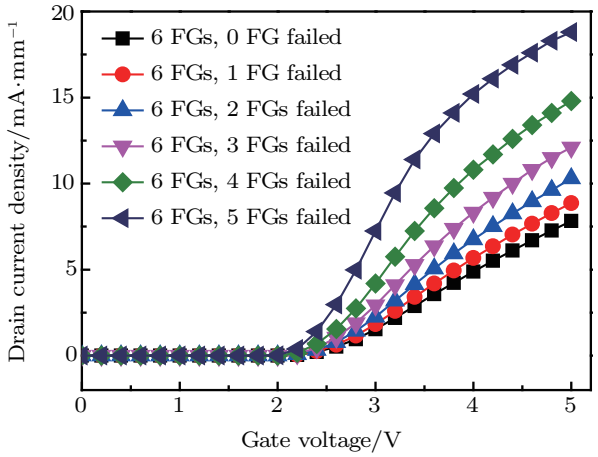


Fig. 5. (color online) Dependence of transfer characteristics on the failure of FGs. 6 FGs with equal 1 μm l_f and equal 0.2 μm s_f is applied. Other parameters are $|n_s| = 5.3\times10^{12}$ cm^{-2}, $|Q_f| = 1.3\times10^{13}$ cm^{-2}, $t_t = 10$ nm, and $t_b = 20$ nm. The TD and BD are both SiO_2. The V_{ds} is 1 V.

Figure 6 shows the influence of l_f on the V_{th} of single FG HEMTs, the l_g was kept as 7 μm. It is seen that as l_f decreased from 7 μm to 1 μm, V_{th} is left shifted gradually. As l_f is less than 1 μm, V_{th} begins to decrease sharply. It is much like the short channel effect.[17] Figure 6 is able to explain the result in Fig. 5 why the V_{th} decreases when FGs failure happened. Figure 6 also shows that the variation tendency was almost the same no matter if $|Q_f|$ is 1×10^{13} cm^{-2} or 1.3×10^{13} cm^{-2}.

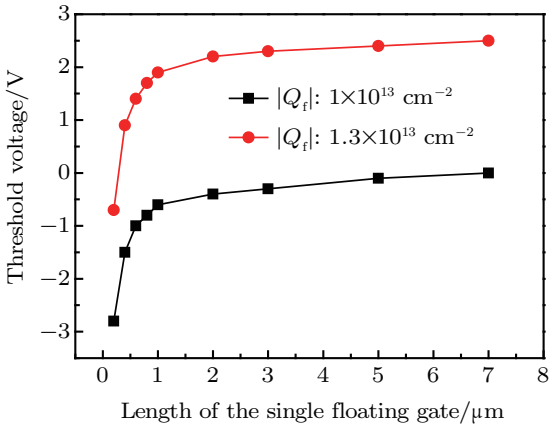


Fig. 6. (color online) V_{th} as a function of l_f for the single FG. The $|n_s| = 5.3\times10^{12}$ cm^{-2}, $t_t = 10$ nm, and $t_b = 20$ nm. The TD and BD are both SiO_2.

According to the Weibull distribution (see Eqs. (5) and (6)),[18] the failure probability of an MIS structure is strongly

related to its area, it can also be used on charge loss of floating gates[19]

$$F_2 = 1-(1-F_1)^{A_2/A_1}, \tag{5}$$

where F_2 is the failure probability of an MIS structure with the area of A_2, F_1 is the failure probability of an MIS structure with the area of A_1.

$$t_1/t_2 = (A_2/A_1)^{1/\beta}, \tag{6}$$

where t_1 is the failure time of an MIS structure with the area of A_1, t_2 is the failure time of an MIS structure with the area of A_2, β is the Weibull slope.

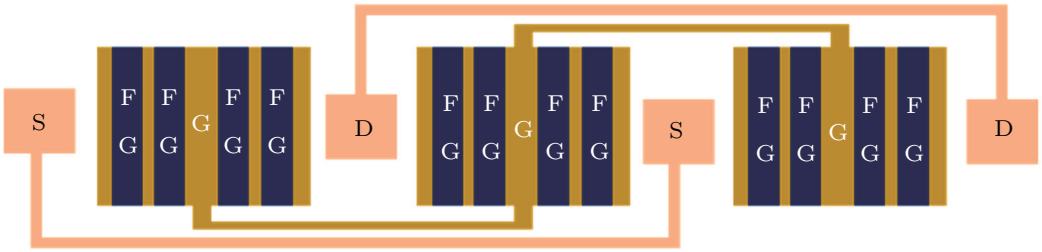


Fig. 7. (color online) The schematic layout (top view) of the multiple finer gates FGs HEMT.

Equation (6) reveals that the smaller area corresponds to longer failure time, indicating that the split FGs HEMT has smaller failure probability in comparison with the HEMT with large area single FG. Furthermore, the control gate can be converted to a certain amount of connected multiple finger gates while each of the FG fingers is separated (Fig. 7). Under the same current rating, the failure probability of the single gate FGs HEMT is calculated to be about Y times higher than the multiple finger gates FGs HEMT according to Eq. (7), in most situations, the calculated result shows $Y \gg 1$.

$$Y = \frac{p_1^m}{C_n^1 p_2^m} = \frac{1}{n}\left(\frac{p_1}{p_2}\right)^m = \frac{1}{n}\left(\frac{1-(1-p_2)^n}{p_2}\right)^m, \tag{7}$$

where n is the finger number, m is the number of FGs on each finger, p_1 is the FG failure probability of the gate, p_2 is the FG failure probability of the multiple gates.

Assuming a 1-A HEMT under drain voltage of 2 V, the on-resistance R is 2 Ω. The R can be calculated by Eq. (8)

$$R = \rho\frac{ml_\mathrm{f}}{nw} = \frac{1}{\mu q|n_\mathrm{s}|}\frac{ml_\mathrm{f}}{nw}, \tag{8}$$

where ρ is the resistivity, w is the FG width, and μ is the mobility.

For AlGaN/GaN HEMT, the typical μ and $|n_\mathrm{s}|$ are 1500 $\mathrm{cm^2\cdot V^{-1}\cdot s^{-1}}$ and 5×10^{12} $\mathrm{cm^{-2}}$, respectively. If the l_g is 7 μm (with 6 FGs, each FG l_f and s_f is 1 μm and 0.2 μm, respectively), the gate width (nw) should be 2.5×10^3 μm. So the gate can be divided to 25 multiple fingers with each finger area of 7 μm×100 μm 6 FGs with each area of 1 μm×100 μm can be prepared on each finger. In flash memory devices of 130-nm technology, the cell failure probability is 5×10^{-6} within 3 years of retention.[20] Assuming that a cell area in the flash memory devices is typical 0.13 μm×0.15 μm = 0.0195 μm^2, the FG (area of 1 μm×100 μm) failure probability was calculated to be 0.025 according to Eq. (5). The failure probability of each finger is 0.025^6=2.5×10^{-10} and the device failure probability was calculated to be 6.3×10^{-9} within 3 years. With the low failure probability, the split FGs structure is shown to be a viable route to E-mode GaN HEMT.

5. Conclusion

In this work, a charge storage-based E-mode AlGaN/GaN split FGs HEMT is proposed and studied by simulations. It is found that the V_th decreases with the increase of 2DEG sheet charge density as well as the tunnel dielectric thickness, while it increases with the increase of FGs sheet charge density and blocking dielectric thickness. The short channel effect was found in the single FG HEMT. The reliability of the device is studied, too. It is found that for 6-FGs HEMT, the reduction of V_th is still moderate when even 5 FGs failed. Moreover, the failure probability of the multiple gates FGs HEMT is calculated to be very low, suggesting that it is a viable route to E-mode GaN HEMT.

References

[1] Luo J, Zhao S L, Mi M H, Chen W W, Hou B, Zhang J C, Ma X H and Hao Y 2016 *Chin. Phys. B* **25** 027303

[2] Chen K J and Zhou C 2011 *Phys. Stat. Soli.* **208** 434

[3] Cai Y, Zhou Y, Lau K M and Chen K J 2006 *IEEE Trans. Electron. Dev.* **53** 2207

[4] Sun W W, Zheng X F, Fan S, Wang C, Du M, Zhang K, Chen W W, Cao Y R, Mao W and Ma X H 2015 *Chin. Phys. B* **24** 017303

[5] Chang C, Pearton S, Lo C, Ren F, Kravchenko I, Dabiran A, Wowchak A, Cui B and Chow P 2009 *Appl. Phys. Lett.* **94** 263505

[6] Hilt O, Brunner F, Cho E, Knauer A, Bahat-Treidel E and Würfl J 2011 *IEEE 23rd International Symposium on Power Semiconductor Devices and ICs (ISPSD)*, 2011, IEEE, p. 239

[7] Lanford W, Tanaka T, Otoki Y and Adesida I 2005 *Electron. Lett.* **41** 449

[8] Ma X H, Pan C Y, Yang L Y, Yu H Y, Yang L, Quan S, Wang H, Zhang J C and Hao Y 2011 *Chin. Phys. B* **20** 027304
[9] Ma X H, Yu H Y, Quan S, Yang L Y, Pan C Y, Yang L, Wang H, Zhang J C and Hao Y 2011 *Chin. Phys. B* **20** 027303
[10] Ota K, Endo K, Okamoto Y, Ando Y, Miyamoto H and Shimawaki H 2009 *IEEE International Electron Devices Meeting (IEDM),* 2009, IEEE p. 1
[11] Lee B, Kirkpatrick C, Yang X, Jayanti S, Suri R, Roberts J and Misra V 2010 *IEEE International Electron Devices Meeting (IEDM),* 2010, IEEE 20.6. 1
[12] Kirkpatrick C, Lee B, Choi Y, Huang A and Misra V 2012 *Phys. Stat. Soli.* **9** 864
[13] Huang H, Liang Y C, Samudra G S and Huang C F 2013 *IEEE 10th International Conference on Power Electronics and Drive Systems (PEDS),* 2013, IEEE p. 555
[14] Zhang Y, Sun M, Joglekar S J, Fujishima T and Palacios T 2013 *Appl. Phys. Lett.* **103** 033524
[15] Pavan P, Bez R, Olivo P and Zanoni E 1997 *Proc. IEEE* **85** 1248
[16] Ťapajna M and Kuzmík J 2012 *Appl. Phys. Lett.* **100** 113509
[17] Awano Y, Kosugi M, Kosemura K, Mimura T and Abe M 1989 *IEEE Trans. Electron. Dev.* **36** 2260
[18] Strong A W, Wu E Y, Vollertsen R P, Sune J, La Rosa G, Sullivan T D and Rauch S E III 2009 *Reliability Wearout Mechanism in Advanced CMOS Technology*, Vol. 12 (New Jersey: John Wiley & Sons)
[19] Belgal H P, Righos N, Kalastirsky I, Peterson J J, Shiner R and Mielke N 2002 *40th Annual Reliability Physics Symposium Proceedings,* 2002, IEEE p. 7
[20] Bez R, Camerlenghi E, Modelli A and Visconti A 2003 *Proc. IEEE* **91** 489